J|A|C|S
ARTICLES
Published on Web 04/08/2004

Synthesis, Structure Solution, Characterization, and Catalytic Properties of TNU-10: A High-Silica Zeolite with the STI Topology

Suk Bong Hong,*,† Emily G. Lear,‡ Paul A. Wright,‡ Wuzong Zhou,‡ Paul A. Cox,§ Chae-Ho Shin,|| Joo-Hyoung Park,⊥ and In-Sik Nam⊥

Contribution from the Division of Chemical Engineering, Hanbat National University, Taejon 305-719, Korea, School of Chemistry, University of St. Andrews, St. Andrews KY16 9ST, United Kingdom, School of Pharmacy and Biomedical Science, University of Portsmouth, Portsmouth PO1 2DT, United Kingdom, Department of Chemical Engineering, Chungbuk National University, Chungbuk 361-763, Korea, and Department of Chemical Engineering, School of Environmental Engineering, Pohang University of Science and Technology, Pohang 790-784, Korea

Received December 28, 2003; E-mail: sbhong@hanbat.ac.kr

Abstract: A high-silica zeolite (Si/Al = 7.1) with the STI framework topology, denoted TNU-10, has been synthesized in the presence of 1,4-bis(*N*-methylpyrrolidinium)butane and Na^+ cations as structure-directing agents, and its structure in the proton form has been refined against laboratory powder X-ray data in space group *Fmmm* ($a = 13.533(1)$ Å, $b = 17.925(2)$ Å, $c = 17.651(2)$ Å). The space group symmetry is supported by electron diffraction and energy minimization studies. The as-made and proton form of TNU-10 are extensively characterized by elemental and thermal analyses, scanning electron microscopy, N_2 adsorption, multinuclear solid-state NMR, IR, and temperature-programmed desorption of ammonia, and the location of the organic structure-directing agent in the channel system is determined by molecular modeling. The catalytic properties of H-TNU-10 and Co-TNU-10 are evaluated for the skeletal isomerization of 1-butene to isobutene and the selective reduction of NO with methane, respectively. When compared to H-ferrierite, a low selectivity to isobutene is observed for H-TNU-10. However, it is found that Co-TNU-10 exhibits a maximum NO conversion of 93% at 823 K under conditions of high concentrations of methane (16000 ppm) and water vapor (10%) and in the presence of 2.6% O_2, which is considerable higher than even the value (74%) obtained from Co-ferrierite, known as the best catalyst for this reaction, under the identical conditions.

1. Introduction

As well as being of considerable scientific interest, the synthesis of zeolites and related microporous materials with novel framework structures or compositions is of technological relevance because of their potential to improve on current technology and to make possible entirely new processes based on catalysis and separation. As a consequence, considerable effort has been devoted over the past decades to generate new zeolitic materials in the presence of the inorganic and/or organic species that act as structure-directing agents (SDAs) in the synthesis mixture.[1]

The natural zeolite stilbite (framework topology code STI) is a medium-pore microporous solid with a pore system delineated by 10-membered rings (free dimensions 4.7 Å × 5.0 Å) connected through 8-membered rings (2.7 Å × 5.6 Å).[2] Two other minerals, stellerite and barrerite, have the framework structure identical to that of stilbite[3] but are characterized by different crystal symmetries, resulting from differences in the number and distribution of extraframework cations. To our knowledge, there are two published synthetic routes to STI-type zeolites, which proceed by the hydrothermal conversion of zeolite laumontite (LAU) or artificial water-free glasses with appropriate oxide compositions in the absence of any organic SDA.[4,5] The Si/Al ratios for all natural and synthetic STI-type materials reported thus far are both narrowly spread (3.3−3.6) and also relatively low,[2−7] and largely as a consequence of the latter, the solids possess only moderate thermal stability. This may be the main reason there has been little work on the catalytic and/or adsorption properties of the STI family of zeolites.

† Hanbat National University.
‡ University of St. Andrews.
§ University of Portsmouth.
|| Chungbuk National University.
⊥ Pohang University of Science and Technology.

(1) International Zeolite Association, Synthesis Commission, http://www.iza-online.org.
(2) Galli, E.; Alberti, A. *Bull. Soc. Fr. Mineral. Cristallogr.* **1975**, *98*, 331.
(3) Treacy, M. M. J.; Higgins, J. B.; von Ballmoos, R. *Collection of Simulated XRD Patterns for Zeolites*; Elsevier: London, 1996.
(4) Liou, J. G., *Contrib. Mineral. Petrol.* **1971**, *31*, 171.
(5) Ghobarkar, H.; Schaef, O.; Guth, U. *J. Solid State Chem.* **1999**, *142*, 451.
(6) Sacerdoti, M.; Sani, A.; Vezzalini, G. *Microporous Mesoporous Mater.* **1999**, *30*, 103.
(7) Li, J.; Qiu, J.; Sun, Y.; Long, Y. *Microporous Mesoporous Mater.* **2000**, *37*, 365.

10.1021/ja031981t CCC: $27.50

Our recent studies of zeolite syntheses using linear diquaternary alkylammonium ions with aliphatic and/or cyclic moieties as organic SDAs have suggested that the conformations of such flexible organic cations could be notably altered according to the nature and extent of interactions with the surrounding inorganic species in synthesis mixtures, which offers a new opportunity for finding new materials.[8−15] Here we present the practical success of this strategy which has enabled us to crystallize a high-silica variant (Si/Al = 7.1) of the STI topology denoted TNU-10,[16] as well as seven other different zeolite structures, from synthesis mixtures with a wide range of gel compositions in the presence of 1,4-bis(*N*-methylpyrrolidinium)butane. This diquaternary ammonium cation has previously been shown to direct the formation of MCM-47, a pure-silica layered material composed of ferrierite (FER) sheets.[17,18] The structure of TNU-10 has been resolved by a combination of laboratory powder X-ray and electron diffraction data, and the physicochemical properties of its as-made and proton forms have been extensively characterized by a number of analytical techniques including elemental and thermal analyses, scanning electron microscopy, N_2 adsorption, IR, ^{13}C, ^{27}Al, and ^{29}Si MAS NMR, molecular modeling studies, and temperature-programmed desorption of ammonia. In addition, we report the catalytic properties of the proton and cobalt-ion-exchanged forms of TNU-10 for the skeletal isomerization of 1-butene to isobutene and the selective reduction of NO with methane in the presence of water, respectively. The catalytic results are compared to those obtained from H-ferrierite and Co-ferrierite that are known to be the best catalysts for these two reactions, respectively.[19,20]

2. Experimental Section

2.1. Zeolite Synthesis. The divalent 1,4-bis(*N*-methylpyrrolidinium)-butane (1,4-MPB) cation was prepared by refluxing 1,4-dibromobutane (99%, Aldrich) with an excess of 1-methylpyrrolidine (97%, Aldrich) overnight in acetone. The excess amine was removed by extraction with acetone, and recrystallizations were performed in methanol−diethyl ether mixtures. The ^{13}C NMR spectrum of the recrystallized 1,4-MPB dibromide (in D_2O) has peaks at 27.5, 28.1, 49.4, 61.7, and 62.8 ppm. Its ^1H NMR spectrum (in D_2O) has peaks at 1.84 (m, 8H), 2.13 (br s, 4H), 2.97 (s, 6H), 3.35 (m, 8H), and 3.45 ppm (br s, 4H). Due to its hygroscopic nature, this diquaternary ammonium salt was stored in a desiccator prior to its use as an organic SDA.

The synthesis of zeolite TNU-10 in the presence of 1,4-MPB was performed using gels prepared by combining NaOH (50% aqueous solution, Aldrich), $Al(NO_3)_3 \cdot 9H_2O$ (98%, Junsei), fumed silica (Aerosil 200, Degussa), and deionized water. The final composition of the synthesis mixture was $4.5R \cdot xNa_2O \cdot yAl_2O_3 \cdot 30SiO_2 \cdot 1200H_2O$, where R is 1,4-MPB, x is varied between $5.0 \le x \le 17.0$, and y is varied between $0 \le y \le 2.0$. When necessary, a portion of NaOH in the gel was replaced by the equivalent amount of KOH (45% aqueous solution, Aldrich). After stirring at room temperature for 1 day, the final synthesis mixture was transferred to Teflon-lined 45-mL autoclaves and heated at 433 K under rotation (100 rpm) for 7−14 days. The solid product was recovered by filtration, washed repeatedly with water, and dried overnight at room temperature. As-made TNU-10 was calcined under flowing air at 823 K for 8 h to remove the occluded organic SDA. The calcined sample was then refluxed twice in 1.0 M NH_4NO_3 solutions for 6 h followed by calcination at 823 K for 2 h to obtain its proton form (i.e., H-TNU-10). Co^{2+}-exchanged TNU-10 (Co-TNU-10) was also prepared by stirring NH_4-TNU-10 twice in 0.02 M $Co(CH_3CO_2)_2$ solutions at 343 K for 12 h followed by calcination in air at 873 K for 2 h.

For catalytic comparison, H-ferrierite (H-FER) and Co-ferrierite (Co-FER) were prepared according to the procedures that are similar to those described above. A Na,K-ferrierite with Si/Al = 8.9 obtained from Tosoh was used as the starting material for ion exchange.

2.2. Analytical Methods. Crystallinity and phase purity of the solids were determined by powder X-ray diffraction (XRD) patterns using a Rigaku Miniflex or a Rigaku 2500H diffractometer with Cu Kα radiation. In situ high-temperature XRD experiments were performed on a Scintag XDS 2000 diffractometer equipped with an Edmund Bühler HDK 1.4 high-temperature attachment. Elemental analysis was carried out at the Analytical Laboratory of the Korea Institute of Science and Technology, using a Jarrell-Ash Polyscan 61E inductively coupled plasma spectrometer in combination with a Perkin-Elmer 5000 atomic absorption spectrophotometer. Thermogravimetric analyses (TGA) were performed in air on a TA Instruments SDT 2960 thermal analyzer, where the exothermic weight loss related to the combustion of organic species was further confirmed by differential thermal analyses (DTA) using the same analyzer. Crystal morphology and size were determined by a JEOL JSM-6300 scanning electron microscope (SEM). The N_2 sorption experiments were performed on a Micromeritics ASAP 2010 analyzer.

For detailed structural analysis a H-TNU-10 sample was loaded into a 0.7 mm quartz glass capillary, connected to a vacuum line and dehydrated for 6 h at 623 K under a vacuum of 4×10^{-4} Torr. The capillary was sealed and analyzed on a Stoe STADI P diffractometer operating in transmission mode (Debye−Scherrer geometry) with primary monochromation and Cu $K\alpha_1$ X-radiation ($\lambda = 1.54056$ Å). Data were collected at ambient temperature with a step size of 0.01° for a scan time of 6 s per step over the range $5° \le 2\theta \le 80°$. Profile refinement of the structure model derived by assigning the *hkl* reflections of the XRD pattern of stellerite (STI topology)[3] to the X-ray peak positions in the pattern of H-TNU-10 was performed by the Rietveld method[21] with the program GSAS.[22] To describe the peak shape, a pseudo-Voigt function[23] was then used together with a manually interpolated background. Constraints on the Si−O distances were used in the first stages and finally removed before the model was refined to convergence. To gain further insight into the possible space groups of H-TNU-10, electron diffraction (ED) and lattice imaging were obtained on a JEOL 2010 transmission electron microscope (TEM) operating at an accelerating voltage of 200 kV. The sample was ground and deposited from a suspension in acetone onto a holey carbon grid. ED patterns were both taken directly onto film and also generated from TEM images using the DigitalMicrograph 3.4.4 software.

The ^{29}Si MAS NMR spectra were measured on a Bruker DSX 400 spectrometer at a spinning rate of 12.0 kHz. The operating ^{29}Si frequency was 79.492 MHz, and the spectra were obtained with an

(8) Paik, W. C.; Shin, C.-H.; Hong, S. B. *Chem. Commun.* **2000**, 1609.
(9) Lee, S.-H.; Lee, D.-K.; Shin, C.-H.; Paik, W. C.; Lee, W. M.; Hong, S. B. *J. Catal.* **2000**, *196*, 158.
(10) Paik, W. C.; Shin, C.-H.; Lee, J. M.; Ahn, B. J.; Hong, S. B. *J. Phys. Chem. B* **2001**, *105*, 9994.
(11) Han, D.-Y.; Woo, A. J.; Nam, I.-S.; Hong, S. B. *J. Phys. Chem. B* **2002**, *106*, 6206.
(12) Lee, S.-H.; Lee, D.-K.; Shin, C.-H.; Park, Y. K.; Wright, P. A.; Lee, W. M.; Hong, S. B. *J. Catal.* **2003**, *215*, 151.
(13) Lee, S.-H.; Shin, C.-H.; Choi, G. J.; Park, T.-J.; Nam, I.-S.; Hong, S. B. *Microporous Mesoporous Mater.* **2003**, *60*, 237.
(14) Lee, S.-H.; Shin, C.-H.; Hong, S. B. *Chem. Lett.* **2003**, *32*, 542.
(15) Lee, S.-H.; Shin, C.-H.; Yang, D.-K.; Ahn, S.-D.; Nam, I.-S.; Hong, S. B. *Microporous Mesoporous Mater.* **2004**, *68*, 97.
(16) Hong, S. B. Korean Patent Appl. 5093659, 2002.
(17) Valyocsik, E. W. U.S. Patent 5068096, 1991.
(18) Burton, A.; Accardi, R. J.; Lobo, R. F.; Falcioni, M.; Deem, M. W. *Chem. Mater.* **2000**, *12*, 2936.
(19) Meriaudeau, P.; Naccache, C. *Adv. Catal.* **1999**, *44*, 505.
(20) Armor, J. N. *Catal. Today* **1995**, *26*, 147.
(21) Rietveld, H. M. *J. Appl. Crystallogr.* **1969**, *2*, 65.
(22) Larson, A.; von Dreele, R. B. *GSAS [General Structure Analysis System] Manual*; Los Alamos Scientific Laboratory Report No. LA-UR-86-748; Los Alamos Scientific Laboratory: Los Alamos, NM, 1986.
(23) Hastings, J. B.; Thomlinson, W.; Cox, D. E. *J. Appl. Crystallogr.* **1984**, *17*, 85.

acquisition of ca. 800 pulse transients, which were repeated with a $\pi/5$ rad pulse length of 2.0 μs and a recycle delay of 60 s. The ^{29}Si chemical shifts are referenced to TMS. The ^{27}Al MAS NMR spectra were recorded on the same spectrometer with a spinning rate of 13.0 kHz at a ^{27}Al frequency of 104.269 MHz. The spectra were obtained with an acquisition of 2048 pulse transients, which were repeated with a $\pi/20$ rad pulse length of 0.5 μs and a recycle delay of 1 s. The ^{27}Al chemical shifts are referenced to an $Al(H_2O)_6^{3+}$ solution. The ^{1}H$-^{13}$C CP MAS NMR spectra at a spinning rate of 4.5 kHz were recorded at a ^{13}C frequency of 100.623 MHz with a $\pi/2$ rad pulse length of 5.0 μs, a contact time of 1 ms, and a recycle delay of 3 s. Approximately 6500 scans were accumulated. The ^{13}C chemical shifts are reported relative to TMS. The IR spectra in the structural region were measured on a Nicolet 360 FT-IR spectrometer using the KBr pellet technique. The IR spectra in the OH region were measured on the same spectrometer using self-supporting zeolite wafers of approximately 15 mg (1.3-cm diameter). Prior to IR measurements, the zeolite wafers were dehydrated at 723 K under vacuum to a residual pressure of 10^{-5} Torr for 2 h inside a home-built IR cell with CaF_2 windows. Temperature-programmed desorption (TPD) of ammonia was recorded on a fixed-bed, flow-type apparatus attached to a Balzers QMS 200 quadruple mass spectrometer, following the procedure described elsewhere.[9]

Lattice energy minimization studies of the isolated TNU-10 framework were performed using the program GULP.[24] A formal charge ionic model was used, with interatomic potentials being used to describe the short-range interactions. Polarization was incorporated via the Shell model, and a three-body term was used to include the effects of directional covalent bonding for the O−Si−O bonds. The parameters used were those reported by Sanders et al.[25] The calculations were performed at constant volume, assuming a pure-silica framework, with the lattice parameters held fixed at the experimentally observed values for both the as-made and proton forms of TNU-10. The optimized coordinates from the lattice energy minimization calculation using the cell parameters of the as-made sample were used in all the subsequent framework−organic SDA calculations. Molecular modeling studies were carried out using a combined Monte Carlo−simulated annealing (MC−SA) approach.[26] In the initial Monte Carlo part of the calculation, the molecule was docked into the lattice at a random position within the unit cell. The energy of the framework−organic interaction was calculated, and the configuration was accepted only if the calculated energy was below 4200 kJ·mol^{-1}; otherwise, the process was started again. Once an initial configuration had been accepted, successive molecular dynamics simulations were performed at 750, 500, 350, and 200 K for 2000 time steps of 1 fs at each temperature, prior to a final energy minimization stage. The framework was held fixed during the simulation, which used the CVFF force field as implemented in the program Discover.[27] This MC−SA cycle was repeated 25 times using a R10000 Silicon Graphics Workstation. The two lowest-energy configurations were further investigated by density functional theory (DFT) to complement the results from the MC−SA simulations by ensuring the electronic feasibility of the locations predicted for the organic SDA. The DFT calculations were performed using CASTEP version 4.2[28] running on a three-node, four-processor (Power 3) IBM RS/6000SP parallel machine. Exchange and correlation energies were calculated using the generalized gradient approximation (GGA) based on the Perdew and Wang functional. Ultra-soft pseudopotentials were used with a kinetic energy cutoff for the plane wave basis set of 260 eV.

2.3. Catalysis. All the catalytic experiments of this study were carried out under atmospheric pressure in a continuous-flow apparatus with a fixed-bed microreactor. Prior to the experiments, the catalyst was routinely activated under flowing He (50 cm^3·min^{-1}) at 773 K for 2 h and kept at the desired temperature to establish a standard operating procedure allowing time for the product distribution to stabilize.

In the skeletal isomerization of 1-butene, a reactant stream with a He/1-butene molar ratio of 9.0 was fed into a quartz reactor containing 0.1 g of zeolite catalyst at 673 K. The total gas flow at the reactor inlet was kept constant at 50 cm^3·min^{-1}. The reaction products were analyzed online in a Chrompack CP 9001 gas chromatograph equipped with an Al_2O_3/KCl Plot capillary column (0.53 mm × 50 m) and a flame ionization detector (FID), with the first analysis carried out after 10 min on stream. Conversion was calculated in terms of the mol % of 1-butene, and selectivity to isobutene was calculated by dividing the isobutene yield by the 1-butene conversion. In the selective reduction of NO by CH_4, a reactant stream consisting of 1200 ppm NO, 2400−16000 ppm CH_4, 2.6% O_2, and 0 or 10% H_2O with He as a balancing gas was fed into a fixed-bed reactor containing 0.65 g of catalyst with a mesh size of 20/50 at a total flow rate of 300 cm^3·min^{-1}, using Brooks 5850E mass flow controllers. The typical gas hourly space velocity (GHSV) was 14000 h^{-1} based on the apparent bulk density of the zeolite catalysts, ca. 0.5 g·cm^{-3}. The reaction products were analyzed by using an online Hewlett-Packard 5890 series II gas chromatograph equipped with a thermal conductivity detector and a Quadstar 422 quadrupole mass spectrometer, and the first analysis was carried out after 4 h on stream. The NO conversion was calculated on the basis of only the N_2 formation, and the CH_4 conversions were obtained by following changes in the CH_4 peak area.

Table 1. Representative Products Obtained Using 1,4-Bis(*N*-methylpyrrolidinium)butane (1,4-MPB) as an Organic SDA[a]

	gel composition			
run	SiO_2/Al_2O_3	$NaOH/SiO_2$	time (days)	product[b]
1	60	1.00	14	TNU-10
2[c]	60	1.00	14	mordenite
3	15	1.00	14	analcime
4	30	1.00	7	TNU-10
5	120	1.00	14	TNU-10
6	240	1.00	14	analcime + (TNU-10)
7	∞	1.00	7	−[d]
8	60	1.13	14	analcime
9	60	0.87	14	IM-5 + TNU-9
10	60	0.73	14	TNU-9
11	40	0.73	7	MCM-22
12	∞	0.73	7	MCM-47
13	60	0.60	7	quartz + ZSM-12
14	60	0.47	7	ZSM-12
15	∞	0.47	7	MCM-47
16	60	0.33	7	ZSM-12 + amorphous
17	60	1.00[e]	7	D[f]
18	60	1.00[g]	7	offretite
19	60	0.73[e]	14	amorphous
20	60	0.73[g]	14	NU-87

[a] The oxide composition of the synthesis mixture is $4.5R{\cdot}xNa_2O{\cdot}yAl_2O_3{\cdot}30SiO_2{\cdot}1200H_2O$, where R is 1,4-MPB, and x and y are varied between $5.0 \le x \le 17.0$ and $0.0 \le y \le 2.0$, respectively. All the syntheses were carried out under rotation (100 rpm) at 160 °C, unless otherwise stated. [b] The product appearing first is the major phase, and the product obtained in a trace amount is given in parentheses. [c] Run performed under static conditions. [d] No solids produced. [e] KOH/SiO_2 ratio. [f] Unknown, probably dense material. [g] $(NaOH + KOH)/SiO_2$ ratio with Na/K = 1.0.

3. Result and Discussion

3.1. Synthesis. Table 1 lists the representative products obtained using 1,4-MPB as an organic SDA from synthesis mixtures with different oxide compositions under the conditions described above. In each case, the phases listed were the only ones obtained in repeated trials. When the $NaOH/SiO_2$ ratio in the gel was fixed to 1.00, as seen in Table 1, we were able to

(24) Gale, J. D. *Faraday Trans.* **1997**, *93*, 629.
(25) Sanders, M. J.; Leslie, M. J.; Catlow, C. R. A. *J. Chem. Soc., Chem. Commun.* **1984**, 1271.
(26) Stevens, A. P.; Gorman, A. M.; Freeman, C. M.; Cox, P. A. *J. Chem. Soc., Faraday Trans.* **1996**, *92*, 2065.
(27) *Discover*, version 99.1; Accelrys: San Diego, U.S.A.
(28) *CASTEP*, 4.2 Academic Version, licensed under the UKCP-MSI Agreement, *Rev. Mod. Phys.* **1999**, *64*, 1045.

crystallize TNU-10 from synthesis mixtures with $SiO_2/Al_2O_3 = 30-120$. However, the synthesis using sodium aluminosilicate gels with $SiO_2/Al_2O_3 < 30$ yielded analcime (ANA) or mordenite (MOR), depending on the period of crystallization time employed. In addition, no solid products were obtained from synthesis mixtures with $SiO_2/Al_2O_3 > 240$ under the conditions described above. Of particular interest is the observation that the phase selectivity of crystallization is very sensitive to the concentration of NaOH in the synthesis mixture. When the initial SiO_2/Al_2O_3 ratio in the gel was fixed to 60, for example, a novel zeolite denoted TNU-9, instead of TNU-10, was formed from a synthesis mixture with $NaOH/SiO_2 = 0.73$. We are carrying out the structure determination of TNU-9 using synchrotron powder XRD and high-resolution TEM data, and the results will be described elsewhere. It should also be noted that a lamellar precursor of MCM-22 (MWW) was the product obtained from a gel with $SiO_2/Al_2O_3 = 40$ and $NaOH/SiO_2 = 0.73$, again revealing the strong influence of Al content in the gel on the product selectivity in the 1,4-MPB-mediated synthesis of zeolites. When the initial $NaOH/SiO_2$ ratio in the synthesis mixture was further decreased to 0.47, on the other hand, ZSM-12 (MTW) and MCM-47 were the phases that crystallized from gels with $SiO_2/Al_2O_3 = 60$ and ∞, respectively. From the synthesis results in Table 1, therefore, it is clear that the oxide composition range yielding pure TNU-10 in the presence of 1,4-MPB is rather narrow. In fact, elemental analysis has indicated that the Si/Al ratios for all the TNU-10 zeolites prepared here are always within the very narrow range of 6.5−7.5. This suggests that there is a specific level of Na^+ ions in the synthesis mixture, and a certain amount of lattice charge, required for the crystallization of TNU-10 using 1,4-MPB.

Table 1 also shows that when the synthesis conditions were selected so that $SiO_2/Al_2O_3 = 60$ and $(NaOH + KOH)/SiO_2 = 1.00$ with $Na/K = 1.00$, offretite (OFF) was the phase formed in the presence of 1,4-MPB. In contrast, we obtained another zeolite, NU-87 (NES), from a gel with $(NaOH + KOH)/SiO_2 = 0.73$ where $Na/K = 1.00$. These results clearly indicate that the combined use of Na^+ and K^+ ions also has great influence on the 1,4-MPB-mediated synthesis of zeolites. The powder XRD patterns of all the materials except analcime (i.e., TNU-10, mordenite, TNU-9, MCM-22, MCM-47, ZSM-12, offretite, and NU-87) prepared in the presence of 1,4-MPB as an organic SDA can be found in Supporting Information Figure 1S. Comparison with the patterns in the literature[3] reveals that they are highly crystalline, and no reflections other than those from the corresponding phases are observed. Also, TGA/DTA experiments indicate that all of them contain significant amounts (>12 wt %) of organic species. Based the overall synthesis results of this study, therefore, it is clear that the structure-directing ability of the linear diquaternary 1,4-MPB ion is not strong enough to dominate over the impact of inorganic gel chemistry, which may in large part be attributed to its high flexibility. This leads us to believe that the types of the conformations of this cation could differ distinctly, according to the nature and extent of interactions with the surrounding inorganic species in synthesis mixtures, making it possible to yield a surprising large variety of different zeolite structures.

3.2. Structure Solution. Figure 1 shows the powder XRD patterns of the as-made and proton forms of TNU-10. Comparison with the patterns of already known zeolite structures

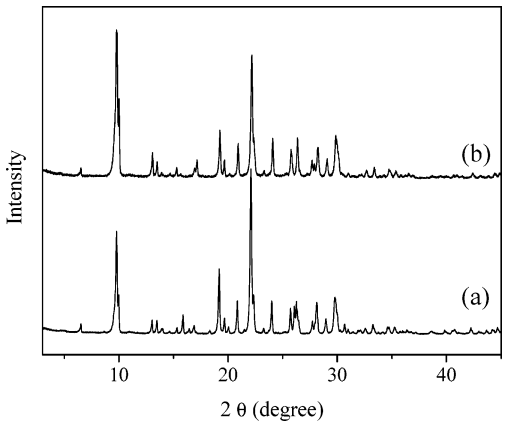

Figure 1. Powder XRD patterns of the (a) as-made and (b) proton forms of TNU-10.

Table 2. Final Atomic Coordinates and Thermal Parameters for H-TNU-10 in *Fmmm* Symmetry with Standard Deviations in Parentheses

atom	*x*	*y*	*z*	U_{iso} (Å^2)
Si(1)	0.3868(5)	0.3124(4)	0.3748(4)	0.021(1)
Si(2)	0.3057(7)	0.4121(4)	0.5000	0.021(1)
Si(3)	0.3876(6)	0.1847(6)	0.5000	0.021(1)
Si(4)	0.2500	0.2500	0.2500	0.021(1)
O(1)	0.3168(6)	0.3038(4)	0.3020(4)	0.024(3)
O(2)	0.3739(9)	0.2365(5)	0.4249(4)	0.024(3)
O(3)	0.3613(8)	0.3844(5)	0.4246(4)	0.024(3)
O(4)	0.5000	0.3219(10)	0.3477(9)	0.024(3)
O(5)	0.3077(8)	0.1169(8)	0.5000	0.024(3)
O(6)	0.3118(16)	0.5000	0.5000	0.024(3)
O(7)	0.5000	0.1536(12)	0.5000	0.024(3)

reveals that the XRD pattern of as-made TNU-10 is very similar to that of stilbite, barrerite, or stellerite.[3] All these natural zeolites possess the same aluminosilicate framework topology (STI) but have different inorganic cation contents and crystal symmetries. Stilbite is monoclinic *C*2/*m*, whereas barrerite (*Amma*) and stellerite (*Fmmm*) are orthorhombic. The pattern of as-made TNU-10 is successfully indexed as orthorhombic, with $a = 13.553$ Å, $b = 18.023$ Å, $c = 17.695$ Å.

The unit cell dimensions of the calcined, dehydrated H-TNU-10 were calculated directly from the powder XRD data and later refined in the GSAS suite of programs as part of the structural analysis to be orthorhombic, $a = 13.534(1)$ Å, $b = 17.925(2)$ Å, $c = 17.651(2)$ Å. For the Rietveld refinement, the framework atomic positions reported for stellerite in the space group *Fmmm* were taken as a starting model. There was no evidence from the XRD data that the symmetry was lower than *Fmmm*. The Si−O bond lengths and O−O distances were constrained to be 1.61 ± 0.03 Å, and the O−O distances within the same tetrahedra were refined to be 2.63 ± 0.05 Å. Thermal parameters were refined, constraining those of silicons to be the same, and also those of all the oxygens to a single value. An acceptable final "goodness-of-fit" value, $R_{wp} = 0.12$, was obtained. The final lattice parameters obtained were $a = 13.5335(10)$ Å, $b = 17.9252(16)$ Å, $c = 17.6507(15)$ Å, $\alpha = \beta = \gamma = 90°$. The final atomic positions are listed in Table 2 with the final Rietveld plot displayed in Figure 2. The average T−O bond length (1.613 Å) and average O−T−O and T−O−T angles (109.47 and 150.6°, respectively) were found to be in good agreement with those expected for zeolitic materials. Attempts to refine the structure in the space group *Amma* (the space group of barrerite)

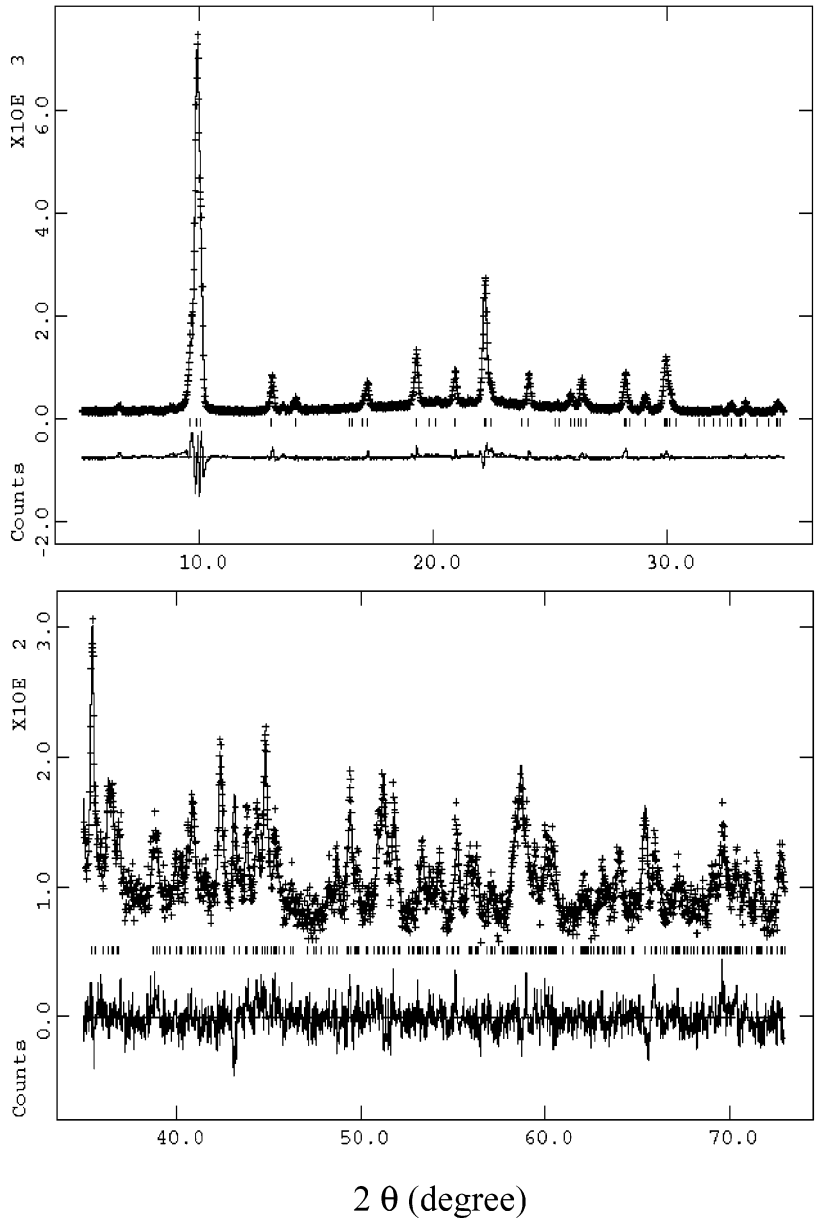

Figure 2. Rietveld plot for H-TNU-10: observed data (+), calculated profile (solid line), and difference (lower trace). The tick marks represent the positions of allowed reflections.

gave no significant improvement in the goodness-of-fit and resulted in chemically unreasonable bond angles. The final refined structure of H-TNU-10, which has the STI framework topology, is shown in Figure 3. The material possesses a pore system comprising gently undulating 10-ring channels along the *a*-axis, themselves linked only through small, elliptical 8-ring openings along the *c*-axis, and separated by framework walls perpendicular to the *b*-axis. Computer simulation of the framework structure in space group *Fmmm* by energy minimization using GULP gave closely similar fractional atomic coordinates for the idealized pure silica framework (see Supporting Information Table 1S). Computer simulation also indicates that allowing the symmetry to reduce from *Fmmm* to *Amma* for the pure-silica polymorph does not result in a lower energy.

The fact that the space group of H-TNU-10 is not lower than *Fmmm* can be further shown by the ED patterns given in Figure 4. The pattern in Figure 4a, taken along the [010] direction, shows some faint intensity for $h \neq 2n$, but this is attributed to multiple scattering from thick samples. As seen in Figure 4b, the ED pattern along the [01−1] direction was also found to be consistent with the space group *Fmmm*. Although the sample was beam sensitive, it was possible to obtain high-resolution TEM images of the material by using very low beam brightness and short exposure time. Figure 4c is a typical image viewed down the [010] zone axis. As well as showing a well-ordered structure, faint modulation along the [101] direction indicates that an incommensurate structural modulation is present. Fourier transformation of the image gives a simulated diffraction pattern with weak maxima along the [101] direction, corresponding to repeat a distance of ca. 20 Å. The fringes in the image that correspond to the superlattice do not cross the whole particle. Although the incommensurate modulation is not as well developed as that observed by Liu et al.[29] in SSZ-24, a pure-silica version of the aluminophosphate molecular sieve $AlPO_4$-5 (AFI), and is therefore difficult to fully characterize, it is

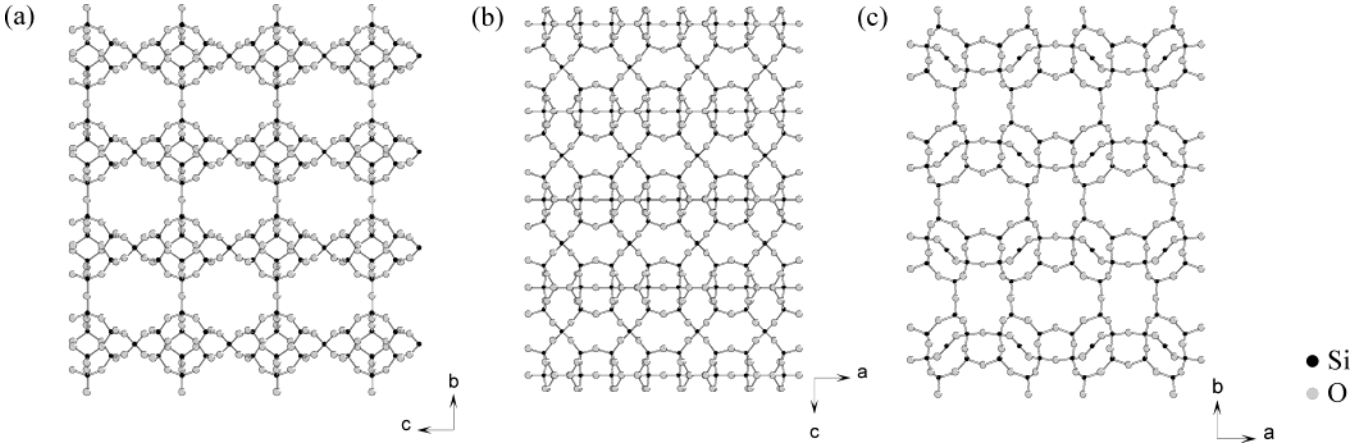

Figure 3. Projections of the finally refined structure of H-TNU-10 along (a) the *a*-axis, (b) the *b*-axis, and (c) the *c*-axis.

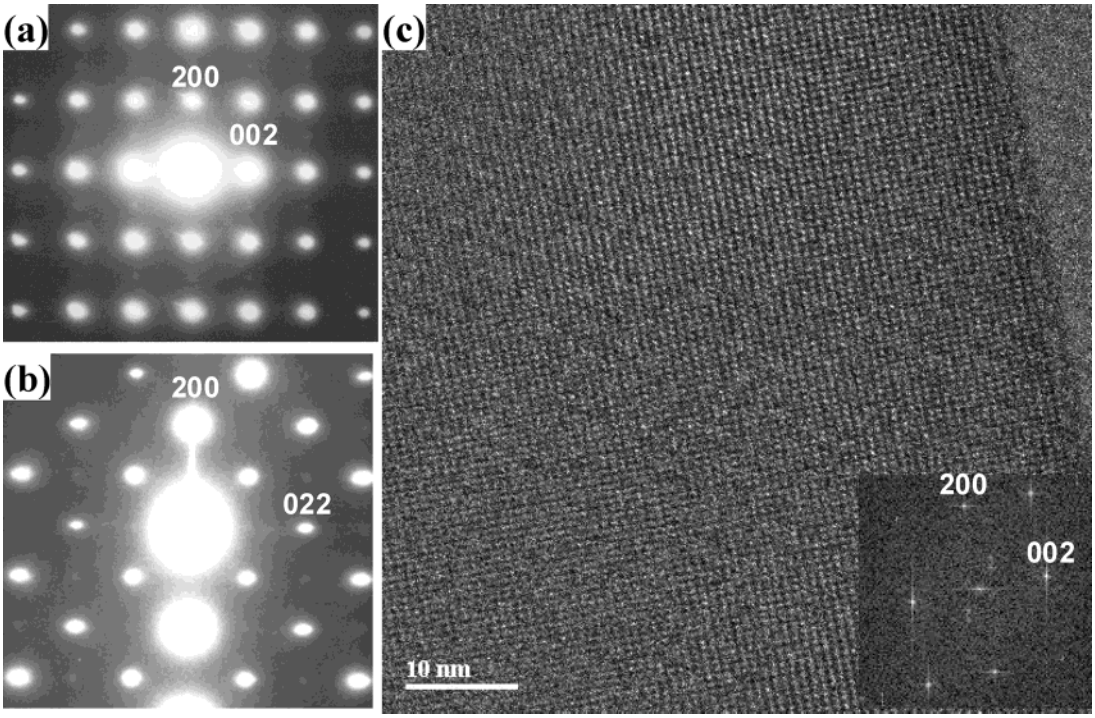

Figure 4. ED patterns of H-TNU-10 along (a) the [010] zone axis and the (b) [01−1] zone axis. (c) Electron micrograph of H-TNU-10 taken down the [010] zone axis. (Inset) Diffraction pattern generated by Fourier transforming this image, revealing spots due to an incommensurate superlattice.

interesting to note that, like the case of SSZ-24, one of the Si−O−Si angles (around O(6); see Supporting Information Table 2S) for the refined H-TNU-10 structure remained unexpectedly high (ca. 174(2)°) for zeolitic materials. This has led us to speculate that the true angle may deviate from the value given above and produce a large period (∼20 Å) of modulation.

3.3. Characterization. As seen in Figure 1, the powder XRD pattern of H-TNU-10 agrees well with that of as-made TNU-10, except for the minor changes in relative X-ray peak intensities and positions, reflecting excellent stability. To further examine the thermal stability of H-TNU-10, we have performed in situ powder XRD experiments under vacuum to a residual pressure of 5×10^{-5} Torr at temperatures up to 1373 K. When the crystallinity was defined as the ratio of areas of the most intense (020) reflection appearing at $2\theta = 9.87°$, in the XRD patterns of H-TNU-10 treated at temperatures higher than 823 K and at this temperature the material heated at 1373 K was found to exhibit ca. 85% crystallinity, which is important for its catalytic applications. From N_2 adsorption experiments on H-TNU-10, the type I isotherm indicates a microporous pore volume of 0.172 $cm^3 \cdot g^{-1}$. The SEM micrograph shows that TNU-10 prepared here appears as agglomerates of heavily overlapped rectangular plates of about $0.5 \times 1.0 \times 0.1$ μm^3 (see Supporting Information Figure 2S). It is noteworthy that the TGA/DTA curves of as-made TNU-10, which can also be seen in Supporting Information Figure 2S, give no signs of decomposition of organic in TNU-10 between room temperature and 723 K, while there is a large weight loss (∼15 wt %) at temperatures up to 973 K accompanied by three exotherms around 745, 810, and 905 K. Such a comparatively high temperature before the onset of exothermic weight loss in the TGA/DTA data suggests the constrained encapsulation of 1,4-MPB within the TNU-10 pores. On the other hand, a combination of elemental and thermal analyses of as-made TNU-10 gives

(29) Liu, Z.; Fujita, N.; Terasaki, O.; Ohsuna, T.; Hiraga, K.; Camblor, M. A.; Diaz-Cabanas, M.-J.; Cheetham, A. K. *Chem.−A Eur. J.* **2002**, *8*, 4549.

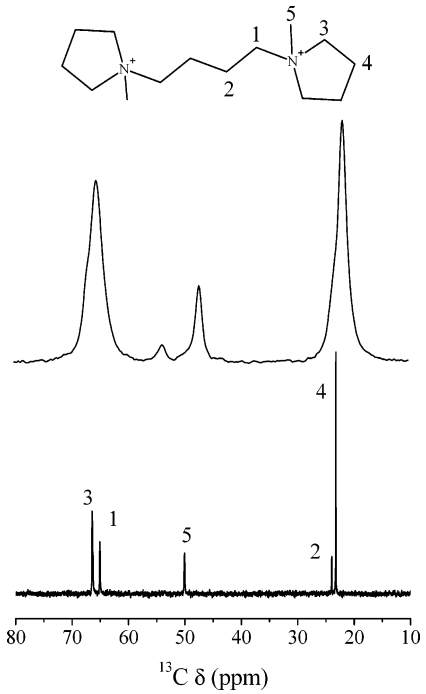

Figure 5. ^{13}C NMR spectra of organic SDA, 1,4-MPB, showing the assignment of each resonance: (a) ^{13}C NMR of 1,4-MPB dibromide in D_2O solution and (b) ^{1}H−^{13}C CP MAS NMR of as-made TNU-10 with 1,4-MPB occluded in the pores.

a unit cell composition of $1,4\text{-MPB}_{3.3}Na_{4.0}Al_{8.9}Si_{63.1}O_{144}\cdot 8.3H_2O$. The higher Si/Al ratio (7.1) of our TNU-10 compared to those for previously reported STI-type zeolites can be explained by the much larger size of the encapsulated 1,4-MPB cations than that of Na^+. The imbalance between the amount of Al and the sum of organic and alkali cations indicates that a fraction of the *N*-methylpyrrolidinium ions occluded within TNU-10 exists as bromide or hydroxide, and serve as space-filling species rather than as charge-compensating cations.

Figure 5 compares the ^{1}H−^{13}C CP MAS NMR spectrum of as-made TNU-10 with the liquid ^{13}C NMR spectrum of the 1,4-MPB dibromide salt. Notice that the resonance of the methyl carbons in the *N*-methylpyrrolidinium rings of 1,4-MPB in as-made TNU-10 splits into two peaks at 53.7 and 47.1 ppm, unlike that of the corresponding carbons of free 1,4-MPB. This implies that two different degrees of geometric constraints and van der Waals interactions with the zeolite framework may be imposed on the methyl groups of the encapsulated 1,4-MPB cations, while the organic SDAs remain intact upon their occlusion into the TNU-10 pores. To gain further evidence to support this speculation, we have attempted to optimize the locations and conformations of the 1,4-MPB in TNU-10 using the MC−SA method followed by energy minimization together with DFT as described above. The lattice constants (*Fmmm*, $a = 13.553$ Å, $b = 18.023$ Å, $c = 17.695$ Å) derived for the as-made TNU-10 were used in these simulations, and the fractional atomic coordinates for the encapsulated organic SDA obtained from the refinement can be found in Supporting Information Table 3S. The lowest-energy conformation for a single 1,4-MPB molecule inside the 10-ring channel of TNU-10 is shown in Figure 6. In this conformation the molecule stretches along the length of the channels that run parallel to the *a*-axis. The methyl groups of the *N*-methylpyrrolidinium end groups point toward 8-ring openings in the side of the channels. Modeling also

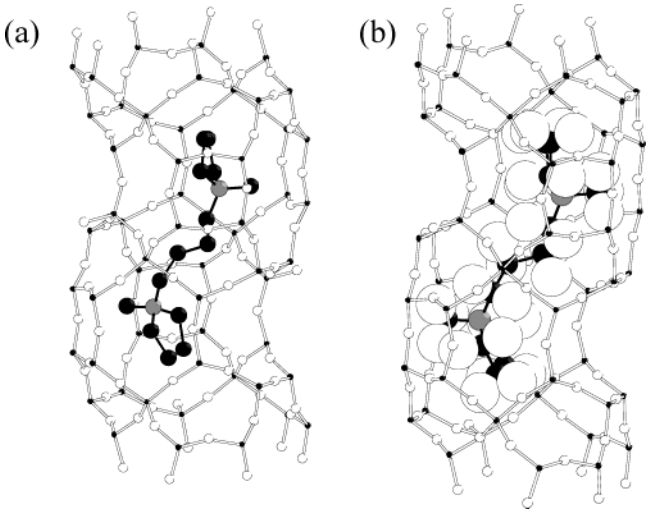

Figure 6. Energy-minimized conformation of the 1,4-MPB molecule within the 10-ring channel of TNU-10. (a) Ball-and-stick model of SDA to emphasize the atom positions and (b) spherical model of SDA to emphasize the efficiency of space-filling of the SDA within the channel.

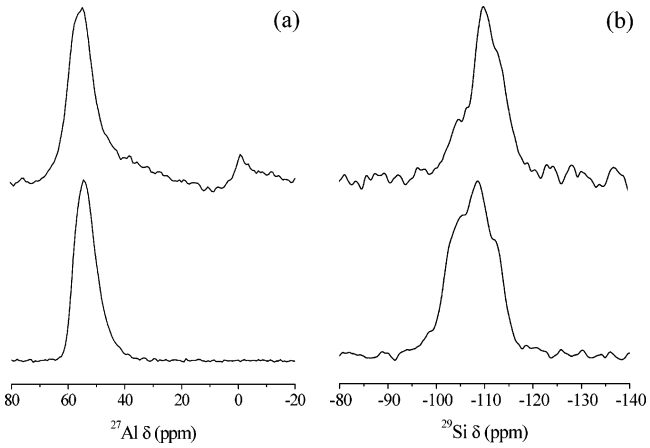

Figure 7. (a) ^{27}Al and (b) ^{29}Si MAS NMR spectra of the as-made (bottom) and proton (top) forms of TNU-10.

reveals locations that are closely similar in energy to this one, in which one *N*-methylpyrrolidinium ring is slightly rotated and the methyl groups no longer point toward the 8-ring. This may explain the splitting into two unequal signals of the methyl resonance of 1,4-MPB in the ^{13}C MAS NMR. The 1,4-MPB is able to pack efficiently within the pore structure of TNU-10, with a maximum predicted filling of four per unit cell, which is somewhat larger than the value (3.3) determined from TGA/DTA. The framework−molecule interaction energy (neglecting Coulombic interactions) per 1,4-MPB molecule with the STI framework was calculated to be -31.2 kJ·mol^{-1}. It should be noted here that this value is only a very little lower than the energies (-24.7 to -30.3 kJ·mol^{-1}) calculated for the molecule within other zeolite structures, such as offretite, ZSM-12, MCM-22, MCM-47, mordenite, and NU-87, all of which were also synthesized with the same organic SDA, i.e., 1,4-MPB. A detailed account of the host−guest interactions occurring within this series of zeolites containing 1,4-MPB as a guest molecule, including the optimized location and conformation of the organic in each zeolite, will be given in a future paper.

Figure 7 shows the ^{27}Al and ^{29}Si MAS NMR spectra of the as-made and proton forms of TNU-10. Only one line around 55 ppm, typical of tetrahedral Al sites, is found in the ^{27}Al MAS

NMR spectrum of as-made TNU-10. However, H-TNU-10 exhibits two additional ^{27}Al resonances: a small line around 0 ppm and a broad shoulder at 30−40 ppm which can be assigned to octahedral and pentacoordinated Al species, respectively.[30] This indicates that a portion of framework Al atoms has been extracted from the TNU-10 framework during the calcination and exchange steps, which can be further supported by comparing the ^{29}Si MAS NMR spectrum of as-made TNU-10 with that of H-TNU-10. Figure 7 reveals a significant difference in the relative intensity of the ^{29}Si resonance around −105 ppm, although both the ^{29}Si MAS NMR spectra are characterized by three main resonances around −112, −109, and −105 ppm. As evidenced by powder XRD and N_2 sorption results, however, it is clear that the overall structural integrity of H-TNU-10 remains intact.

The IR spectrum of as-made TNU-10 in the structural region was found to be very similar to that reported by Li et al. for the calcium-rich, natural zeolite stellerite with Si/Al = 3.2[7] (see Supporting Information Figure 3S). However, there are significant blue shifts in the spectrum of as-made TNU-10, which is in good agreement with its enhanced Si/Al ratio. This is particularly true for the most intense asymmetric stretching band (1052 cm^{-1} for as-made TNU-10; 1035 cm^{-1} for stellerite[7]). Such blue shifts of IR bands are also clear for the case of H-TNU-10. For example, this material gives the asymmetric stretching band at 1072 cm^{-1}, again confirming that partial dealumination has occurred during the SDA removal and successive NH_4^+ ion exchange and recalcination steps to prepare H-TNU-10. On the other hand, the IR spectrum (not shown) of dehydrated H-TNU-10 shows three well-resolved bands around 3745, 3666, and 3608 cm^{-1} in the OH stretching region. The first band is attributed to silanol groups on the external surface of H-TNU-10 crystallites, and the other two bands can be assigned to hydroxyl groups belonging to extra-framework Al and to those of the Brønsted acid sites, respectively.[31] To more accurately characterize the acidic properties of H-TNU-10, we have attempted to measure the IR spectra after pyridine adsorption. However, it was found that pyridine was not readily adsorbed at room temperature on the dehydrated material, probably due to the small size (4.7 Å × 5.0 Å) of the 10-ring channels in H-TNU-10 which significantly restricts the free diffusion of the probe molecules into the intracrystalline acid sites. Thus, the NH_3 TPD on H-TNU-10 has been performed and is given in Figure 8. Included for comparison is the NH_3 TPD profile obtained from H-FER. Both the TPD profiles in Figure 8 are characterized by two desorption peaks, with maxima in the temperature regions 430−460 and 660−710 K, due to NH_3 desorption from weak and strong acid sites, respectively. As expected from their Al contents, the total area of NH_3 desorption (i.e., the density of acid sites) was found to be slightly higher for H-TNU-10 than for H-FER. As seen in Figure 8, however, a considerably lower number of strong acid sites is observed for the former zeolite, which can be attributed partly to the structural differences between these two medium-pore zeolites.

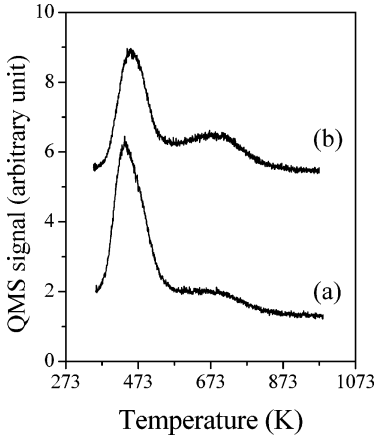

Figure 8. NH_3 TPD profiles from (a) H-TNU-10 and (b) H-FER.

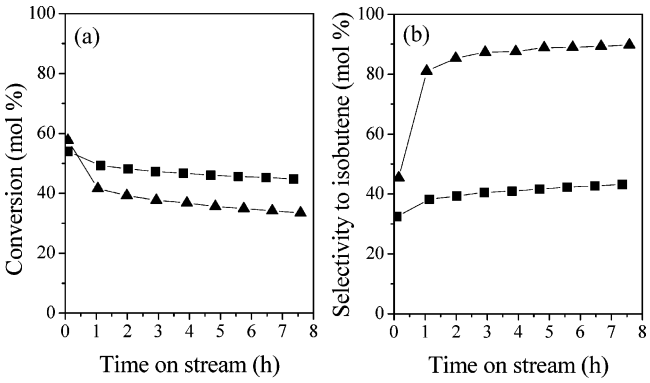

Figure 9. (a) 1-Butene conversion and (b) selectivity to isobutene as a function of time on stream in skeletal isomerization of 1-butene over H-TNU-10 (■) and H-FER (▲) at 673 K and 10.1 kPa 1-butene pressure.

3.4. Catalysis. As described thus far, TNU-10 is a high-silica analogue of the STI family of zeolites whose pore structure consists of two intersecting 10- and 8-ring channels, like that found in FER. While the 10-ring channels (4.7 Å × 5.0 Å) in TNU-10 are less elliptical than the analogous channels (4.2 Å × 5.4 Å) in FER, however, the opposite is observed for the 8-ring channels (2.6 Å × 5.7 Å vs 3.5 Å × 4.8 Å) in these two medium-pore materials.[32] Since H-FER and Co-FER are known to be among the most active catalysts for the skeletal isomerization of 1-butene to isobutene and the selective reduction of NO with CH_4, respectively,[19,20] it is of interest to investigate the performance of H-TNU-10 and Co-TNU-10 as catalysts for these two reactions.

Figure 9 shows 1-butene conversion and selectivity to isobutene as a function of time on-stream in the skeletal isomerization of 1-butene over H-TNU-10 and H-FER measured at 673 K and 10.1 kPa 1-butene in the feed. The results obtained at 5 min on-stream may be regarded as the intrinsic activities of these two zeolites, minimizing the well-known effects of coke deposition within the zeolite pores on the selectivity to isobutene.[12,19,33] As seen Figure 9, H-TNU-10 gives a lower initial selectivity to isobutene (32% vs 46%) than H-FER-10. Furthermore, with increasing time on-stream the selectivity to isobutene over H-TNU-10 remains almost unchanged over the period of time on-stream studied here, whereas the selectivity over H-FER increases. These results show that the pore structure

(30) Engelhardt, G.; Michel, D. *High-Resolution Solid State NMR of Silicates and Zeolites*; Wiley: New York, 1987; p 143.
(31) Karge, H. G.; Hunger, M.; Beyer, H. K. In *Catalysis and Zeolites: Fundamentals and Applications*; Weitkemp, J., Puppe, L., Eds.; Springer: Berlin, 1999; p 198.
(32) International Zeolite Association, Structure Committee, http://www.iza-structure.org.
(33) van Donk, S.; Bitter, J. H.; de Jong, K. P. *Appl. Catal., A* **2001**, *212*, 97.

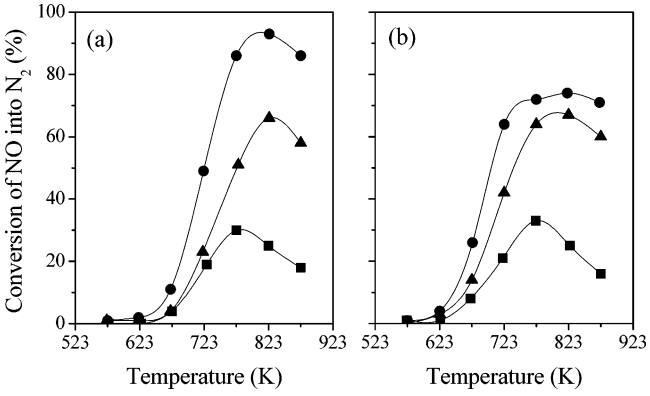

Figure 10. NO conversion to N_2 as a function of temperature in selective reduction of NO over (a) Co-TNU-10 and (b) Co-FER measured at different inlet CH_4 levels of 2400 (■), 8000 (▲), and 16000 (●) ppm. The reactions were run with a feed containing 1200 ppm NO, 2.6% O_2, and 10.0% H_2O at a GHSV of 14000 h^{-1}.

of TNU-10 itself is not efficient for selectively isomerizing 1-butene to isobutene. Very recently, we have investigated the catalytic properties of a series of 10-ring zeolites (i.e., clinoptilolite, FER, ZSM-22, SUZ-4, ZSM-57, and ZSM-5) with different framework structures for this reaction and found that the initial isomerization activity of each zeolite catalyst can be nicely correlated with its 10-ring pore shape.[34] When the ellipticity (ϵ) defined by $\{(b^2 - a^2)/b^2\}^{0.5}$,[35] where a and b are the shortest and longest pore diameters, respectively, is taken as a quantitative measure of differences in the 10-ring pore shape, the ϵ value of 10-ring channels in H-TNU-10 was calculated to be 0.341 which is considerably lower than the value (0.629) of the analogous channels in H-FER. Assuming that the 10-ring pores in H-TNU-10 and H-FER are ideally elliptical in shape, in contrast, the difference in their pore areas (18.4 $Å^2$ vs 17.8 $Å^2$) was found to be negligible. Therefore, we believe that the nonselective behavior of H-TNU-10 for isobutene formation may originate primarily from the shape of its 10-ring channels which are more circular in cross section than those of H-FER. This may allow the intracrystalline space of this STI-type zeolite to more efficiently accommodate *n*-butene molecules, increasing the probability of collisions with other reactant molecules that give rise to side reactions such as dimerization followed by cracking to light hydrocarbons. If such is the case, then these results constitute another example where the catalytic shape selectivities of zeolites and related microporous materials vary strongly with a small variation in their pore shapes.

Figure 10 shows NO conversion to N_2 as a function of reaction temperature in the selective reduction of NO over Co-TNU-10 and Co-FER measured at 14000 h^{-1} GHSV, 1200 ppm NO, 2400−16000 ppm CH_4, 2.6% O_2, and 10% H_2O in the feed. Elemental analysis indicates that the Co contents in Co-TNU-10 and Co-FER are 4.4 and 3.7 wt %, respectively. Taking into account their Al amounts in the framework, thus, both zeolites are characterized by similar Co/Al ratios (0.44 vs 0.51). When the concentration of CH_4 in the feed is fixed to 2400 ppm, Co-FER exhibits a maximum NO conversion of 35% at 773 K under wet conditions, and its conversion decreases at temperatures higher than 773 K. Such a decrease in NO conversion with increasing temperature can be attributed to the impact of CH_4 combustion[20] and is also observed for Co-TNU-10. However, the maximum NO conversion over Co-TNU-10 at the same inlet CH_4 concentration (2400 ppm) was found to be 30% at 773 K, which is smaller than the value observed for Co-FER. The observation that, with increasing CH_4 concentration from 2400 to 16000 ppm, the maximum NO conversion over Co-TNU-10 increases from 30 to 93% while the temperature at which the NO conversion reaches a maximum shifts from 773 to 823 K is of particular interest. As seen in Figure 10, however, Co-FER gives a maximum NO conversion of 74% at 823 K and 16000 ppm CH_4 in the feed. Typically, the real flue gas stream contains a large amount of water vapor as a combustion product. Thus, water tolerance is a critical requirement for the development of a practical deNO_x catalyst, which is a serious drawback of metal-containing zeolites in terms of their applications to this end.[20,36] When examining the activity of Co-TNU-10 for NO reduction by CH_4 under dry conditions, we obtained a much higher NO conversion (54%) for 2400 ppm CH_4 at 723 K. Thus, there is a severe loss in the NO reduction activity of Co-TNU-10 with the introduction of 10% water vapor into the reactant stream, which is consistent with the trend found in most, if not all, of the zeolite-based deNO_x catalysts reported thus far.[37] However, this does not appear to be the case for the reaction of mixtures including a high concentration of CH_4 (16000 ppm), since Co-TNU-10 yields a maximum NO conversion of 84% at 773 K under dry conditions (see Supporting Information Figure 4S). To the best of our knowledge, the NO conversion (93%) of Co-TNU-10 obtained at 823 K and with 16000 ppm CH_4 and 10% water in the feed is higher than those previously reported for metal-containing zeolites, using CH_4 as a reductant under wet conditions. We speculate that at temperatures lower than 723 K this may result from the higher collision probability of CH_4 with NO_x inside the TNU-10 pores upon increasing CH_4 concentration in the feed. At temperatures above 723 K, in contrast, it appears that steam reforming of CH_4 to produce H_2 and CO (which may take place over the cobalt species in TNU-10) is the main reason for the enhancement of NO reduction. A combination of gas chromatography and quadruple mass spectroscopy has revealed the presence of H_2 and CO in product streams, where the former product may also play a role during the NO reduction over Co-TNU-10 at elevated temperatures under the wet conditions described above. We also found that the concentrations of both products reach their maxima at 823 K, which corresponds to the change in NO removal activity. To more accurately elucidate the origin of the remarkable NO removal activity observed for Co-TNU-10 at an extremely high CH_4 level in the presence of water, extensive characterizations of the cobalt species in this STI-type zeolite using UV−vis, X-ray photoelectron, and Co K-edge X-ray absorption spectroscopies, together with testing the NO reduction activities of Co-TNU-10 zeolites with different Co-loading levels, are currently underway in our laboratory. From the catalytic results in Figure 10, however, it is clear that the pore structure is a crucial factor influencing the NO removal activity of metal ion (Co^{2+}, Cu^{2+}, or Mn^{2+})-zeolite-based catalysts, and specifically that Co-TNU-10 is a promising deNO_x catalyst.

(34) Lee, S.-H.; Shin, C.-H.; Hong, S. B. *J. Catal.* **2004**, *223*, 200.
(35) Beyer, W. H. *CRC Standard Mathematical Tables*, 28th ed.; CRC: Boca Raton, FL, 1987.
(36) Li, Y.; Armor, J. N. *Appl. Catal., B* **1993**, *3*, L1.
(37) Traa, Y.; Burger, B.; Weitkamp, J. *Microporous Mesoporous Mater.* **1999**, *30*, 3.

4. Conclusions

The synthesis, structure solution, characterization, and catalytic properties of TNU-10, a high-silica zeolite with the STI topology, have been reported. When the 1,4-bis(*N*-methylpyrrolidinium)butane is used as an organic SDA together with Na^+ ions, pure TNU-10 crystallizes from the synthesis mixture with a relatively narrow range of SiO_2/Al_2O_3 and $NaOH/SiO_2$ ratios. The framework structure of TNU-10 was determined using the laboratory powder X-ray and electron diffraction data. The material possesses a two-dimensional pore system, consisting of gently undulating 10-ring channels intersected by small, elliptical 8-ring openings, which is essentially identical to that reported for the stilbite-type zeolites. A combination of thermal analyses, ^{13}C NMR, and energy minimization calculations reveals a tight encapsulation of the 1,4-bis(*N*-methylpyrrolidinium)butane molecules within the 10-ring channel of TNU-10, imposing upon them a narrow range of conformations. Despite its relatively low Si/Al ratio (7.1), the proton form of TNU-10 (H-TNU-10) exhibits a high thermal stability and is therefore suitable as a catalyst. The catalytic properties of this zeolite for the skeletal isomerization of 1-butene to isobutene are compared to those obtained from H-ferrierite, which has similar pore architecture but slightly different pore sizes and shapes. H-TNU-10 exhibits a lower selectivity to isobutene, which we attribute to the more circular cross section of its 10-ring channels. In the selective reduction of NO with a large excess of methane and in the presence of water, by contrast, the cobalt-exchanged form of TNU-10 was found to give higher NO removal activity than the corresponding cation form of ferrierite, which renders it potentially useful as a $deNO_x$ catalyst for stationary combustion sources.

Acknowledgment. Funding for this work was partially provided by the Korea Science and Engineering Foundation under Grant No. R02-2003-000-10087-0 to S.B.H. We thank Mr. S.-H. Lee (CNU/HNU) for technical assistance.

Supporting Information Available: Additional information as noted in the text (PDF). This material is available free of charge via the Internet at http://pubs.acs.org.

JA031981T